

Turing patterns and solitary structures under global control

L.M. Pismen

Department of Chemical Engineering,

Technion – Israel Institute of Technology, 32000 Haifa, Israel

()

Abstract

Striped Turing patterns and solitary band and disk structures are constructed using a three-variable multiscale model with cubic nonlinearity and global control. The existence and stability conditions of regular structures are analysed using the equation of motion of curved boundaries between alternative states of the short-range component. The combined picture of transitions between striped and spotted patterns with changing level of global control is in qualitative agreement with the results of the computer experiment by Middy and Luss [15].

82.20.Mj, 05.70.Ln

arXiv:patt-sol/9608007v1 20 Aug 1996

I. INTRODUCTION

Stationary patterns of chemical activity (Turing patterns), have attracted wide attention both as a key to understanding complex and unusual phenomena in chemical and electrochemical kinetics and as a possible basis of morphogenesis and biological diversification [1–3]. Similar patterns, emerging as a result of spontaneous symmetry breaking have been known and intensively studied long before that in fluid mechanics [4,5].

Reproducing stationary chemical patterns in the laboratory under controlled conditions turned out to be a rather elusive task, as most observations, such as the BZ reaction, produced propagating chemical waves rather than stationary structures; immobilization of chemical waves was achieved only due convective effects [6] or imposed spatial gradients in the Couette reactor [7,8]. In recent years, novel experimental techniques were applied to obtain a variety of complex chemical patterns in gel reactors [9–12] and on catalytic surfaces [13]. A parallel progress in computing and visualization is evident in $2d$ patterns obtained in recent computer experiments [14,15].

Most common models of large-amplitude dynamics, such as the FitzHugh – Nagumo equation, favor propagating waves, rather than stationary patterns. A basic mechanism generating stationary inhomogeneities is a combination of a short-range activator and a long-range inhibitor with a sufficiently fast dynamics [16]. Formation of chemical patterns can be understood analytically when characteristic spatial and temporal scales associated with different reactants and other dynamic variables, like temperature or potential, are widely separated; this is typical to heterogeneous reacting systems, due to great disparities in diffusion rates. This scale separation allows to use rational approximation techniques, first of all, the method of matched asymptotic expansions, to build up and investigate dynamically complex non-equilibrium patterns [17,18].

The basic element of a non-equilibrium pattern in a multiscale system is a propagating front, or kink, separating regions of prevailing alternative stationary states of the short-range subsystem, usually characterized by a low or high level of the activator. More complex patterns are constructed by allowing other constituents, varying on a longer spatial scale,

to modify the motion of kinks and to mediate their interaction, thereby leading to the formation of bound pairs, trains, etc. Generically, the kinks are “*fast*”, i.e. propagate with a speed of the same order of magnitude as a “unit” speed that can be conjectured from the characteristic length and time scales of the short-range activator. Wave patterns (with relaxation oscillations at any fixed point) are constructed as trains of fast kinks separated by distances far exceeding their width.

Stationary or slowly evolving structures can be “assembled” in a similar way but using as basic elements “*slow*” kinks propagating with a speed much less than unity. The slowing-down can be either a consequence of a symmetry that is only weakly broken due to the influence of long-range fields, or a result of a dynamic adjustment to changing levels of a long-range variable. A Turing pattern can take the form of alternating domains separated by immobilized kinks.

Dynamics of kinks is sensitive to the influence of *global* variables which are present in some of the most common laboratory set-ups. In experiments with catalytic wires [19,20], the global control is due to heating input regulated to keep the average wire resistance (i.e. essentially the average temperature) constant. If local kinetics is bistable, the global control of this kind causes spontaneous symmetry breaking on a global scale [21] due to immobilization of kinks. In electrochemical experiments [22,23] or glow discharge devices [24], the global controlling factor is the conservation of the total current. In both catalytic and electrochemical studies, oscillatory local kinetics, that would normally lead to a pattern of *propagating* waves (or coupled fast kinks) in a distributed system, generates *standing* waves under conditions of global control. Still more complex dynamics of pulses and kinks was obtained in numerical experiments [25].

A different kind of global control is connected with the influence of a rapidly mixed gas phase in catalytic reactions. Recent model computations [26] indicated that a global gas-phase oscillation was the factor causing transition to standing waves in the experiments of the group of Ertl [13]. Global interaction through the gas phase is usually detrimental to pattern formation, as it tends to synchronize the reaction on the entire surface. Recent computations by Middy and Luss [15] demonstrated a sequence of transitions from striped

to spotted patterns and, eventually, to restoration of spatial homogeneity with an increased level of global control.

The main purpose of this communication is to find analytic criteria for such transitions in a reaction-diffusion system with separated scales. Our description of Turing patterns is mainly based on representing them as collections of “solitary” band or disk structures, although we shall also consider regular striped patterns. Different objects bounded by kinks can be indeed viewed as solitary even at moderate distances, since interaction of kinks decays exponentially with separation.

The motion of a slow kink is influenced by its geometric form even when its curvature is small. This distinguishes them from fast kinks, which are insensitive to the geometry unless their curvature radius becomes comparable to their width. Solitary structures bounded by slow kinks are stabilized by a delicate balance between the geometric factors and the influence of long-range variables, and their existence and stability conditions are strongly dependent on their geometric shape.

In the following, we shall consider only slowly evolving structures that are built up of slow kinks, and have a characteristic scale far exceeding the width of the kink. The basic three-variable model with cubic nonlinearity is formulated in Section II, and the equation of motion of a bent kink is derived in Section III. We proceed with the construction of various stationary structures in Section IV, and the analysis of their stability in Section V. The combined picture of the existence and stability regions of solitary band and disk solutions, as discussed in the last Section, is in qualitative agreement with the results of the computer experiment by Middy and Luss [15].

II. BASIC EQUATIONS

A. Reaction-diffusion model with separated scales

The influence of global control variables on the formation of stationary non-equilibrium patterns can be understood qualitatively within the common context of pattern formation in reaction-diffusion systems with separated scales. The common recipe for a stationary

pattern [16–18] calls for a pair of equations for two reacting and diffusing species: a short-range “activator” u and a long-range “inhibitor” v :

$$\gamma u_t = \epsilon^2 \nabla^2 u + f(u, v), \quad (1)$$

$$v_t = \nabla^2 v + g(u, v). \quad (2)$$

The equations are written using the characteristic time and length scales of the long-range component as basic units. The small parameter ϵ is the square root of the ratio of diffusivities of the two species. It is supposed that the nonlinear function $f(u; v)$, with v considered as a parameter, has three zeroes within a certain range of v , two of them, $u = u^\pm(v)$, being stable, and one unstable. Under these conditions, Eq.(1) has propagating kink solutions that separate regions with prevailing “lower” and “upper” states. Everywhere except in an $O(\epsilon)$ vicinity of the kink, the dynamics of v is defined by a closed reaction-diffusion equation

$$v_t = \nabla^2 v + h^\pm(v) \quad (3)$$

with a discontinuous source function given by alternative forms $h^\pm(v) = g(u^\pm(v), v)$ in alternative regions separated by a kink. It is clear that most of the information carried by the function $g(u, v)$ is irrelevant. Its only essential property is reflected by the disposition of null isoclines, i.e loci of zeroes of the functions $f(u, v)$ and $g(u, v)$ in the plane (u, v) , which can be either *synclinal*, as in Fig. 1a, or *anticlinal*, as in Figs. 1b,c.

When the disposition is anticlinal, stable global stationary states satisfying $h^\pm(v) = 0$ may either disappear altogether, as in Fig. 1b, or become *excitable*, as in Fig. 1c. An excitable state $u = u^\pm(v)$ retreats when placed in contact with an alternative steady state of the the short-scale equation $u = u^\mp(v)$ at the same value of v . An advancing front of the alternative state is arrested when the level of the inhibitor adjusts to shifts in the front position, and relaxes to the value $v = v_s$ satisfying the stationarity condition for the kink:

$$I(v_s) \equiv \int_{u_-(v_s)}^{u_+(v_s)} f(u, v_s) du = 0. \quad (4)$$

An immobilized kink-antikink pair forms a solitary structure on the background of an excitable state. Such structures were constructed with the help of a multiscale model with piecewise-linear kinetics [27], and, recently, detected experimentally in gel reactors [12]. A

regular array of alternating kinks and antikinks forms a Turing structure, which is the only stable stationary state in the “oscillatory” case corresponding to the disposition of null isoclines in Fig. 1b.

Stability of immobilized kink structures under conditions when the level of the inhibitor adjusts momentarily to shifts in the position of kinks can be supported by the following qualitative argument. We take note that, when the disposition of null isoclines is anticlinal, as in Fig. 1b,c, v is depleted in the lower state u^- and produced in the upper state u^+ , while, on the contrary, the lower state advances at higher, and the upper, at lower values of v . Consider, for example, a finite region with $u = u^-$ immersed in a continuum with $u = u^+$. If it starts to shrink, the level of v would raise and, as a result, the kinks bounding the region would be immobilized again (a more precise analysis, taking also into account the local gradient of v and effects of the kink curvature is given in Section V). The same argument proves that immobilized fronts should be unstable when the disposition of null isoclines is synclinal, as in Fig. 1a, so that the lower state advances at lower, and the upper, at higher values of v .

B. Global control

The above qualitative arguments can be extended to the case when v is a *global* controlling variable. The model with global interactions can be viewed as a limiting case of the model with separated scales, which is obtained when the diffusivity of the long-range variable tends to infinity, so that its diffusional length far exceeds the size of the system. Then Eq. (2) is replaced by the integral equation

$$v_t = \langle g(u, v) \rangle, \quad (5)$$

where $\langle \dots \rangle$ denotes averaging over the entire reactive surface. The respective form of eq. (3) is

$$v_t = \alpha h^-(v) + (1 - \alpha)h^+(v), \quad (6)$$

where α is the fraction of the surface occupied by the lower state.

The action of either a long-range or a global inhibitor leads to the formation of stable inhomogeneous structures in the case of an anticlinal (but not a synclinal) disposition of null isoclines. The only distinction lies in the characteristic size of the inhomogeneities (either a wavelength of a regular pattern or a width of an excited domain). This size is, generally, determined by the diffusional length of the inhibitor, and increases to become comparable with the size of the system in the case of a global control. Under conditions of global control, the size of inhomogeneities is not limited, and the system evolves to minimize the length of the boundary between the domains with prevailing alternative states. Each disjoint domain tends to become circular as its circumference shrinks due to the line tension of a bounding kink. Further decrease of the length of the boundaries is caused either by the coalescence of domains, or by dissolution of smaller and growth of larger domains under the constraint of a conserved total area. This process is similar to spinodal decomposition in equilibrium systems described by the Cahn – Hilliard equation [28]. Its driving force is either the attractive interaction between like domains, which decays exponentially at a distance comparable with the diffusional length of the short-range variable, or the line tension, which causes the kinks to move with a velocity proportional to the ratio of the same diffusional length to the local curvature radius. As in equilibrium systems, the “ripening” process becomes exceedingly slow as the prevailing size of the extant domains increases.

Separation into domains with prevailing alternative steady states in an anticlinal system is the basis of the “global regulator” model of spontaneous symmetry breaking [21]. This mechanism works, for example, in a catalytic wire heated by electric current when the controls are adjusted to keep the average temperature within the unstable region between the lower (extinct) and higher (ignited) states. In this case, a simple suitable form of the model equations is

$$\gamma u_t = \epsilon^2 \nabla^2 u + F(u) + U, \quad U = B(u_s - \langle u \rangle), \quad (7)$$

which corresponds to an anticlinal disposition. The short-range variable u can be identified as temperature and the global variable U , as the overall heating rate. The disposition would not change qualitatively in a more precise model taking into account the dependence of local heat dissipation on local temperature.

The situation is different when the global control is caused by the interaction with a rapidly mixed ambient fluid phase that changes its composition and/or temperature in response to the changes of the averaged state of the catalytic surface. The simplest model suitable to this case is

$$\gamma u_t = \epsilon^2 \nabla^2 u + F(u) + U, \quad U_0 - U = B(U - \langle u \rangle), \quad (8)$$

where U has now the meaning of concentration or temperature in the ambient fluid. In this case, the disposition of null isoclines is *synclinal*, and no symmetry breaking occurs. If other factors induce formation of Turing patterns or excitation domains on the catalytic surface, the global interaction of this kind acts to modify the emerging patterns, and may suppress them altogether when it is sufficiently strong.

C. Three-variable model with a cubic nonlinearity

In the following, we shall consider a minimal model including three variables: a short-range activator u , a long-range inhibitor v , and a global controller of the synclinal type U that suppresses pattern formation. Analytical studies of non-equilibrium patterns often employ equations with a discontinuous piecewise linear source function for a *short-range* variable, as this form of the source function makes computations most simple. Such a model was used, in particular, to construct stationary structures as immobilized pairs or arrays of kinks [27]. In any physical situation discontinuous source functions can only appear when there is some hidden short-range variable that has been removed using a procedure of the same kind that has lead us from Eq.(2) to Eq.(3). In the long-range equation, however, the position of the discontinuity is not free but has a dynamics of its own, dependent on the dynamics of the short-range variable in the kink region. If this dynamics is ignored, and a discontinuous function is used in the basic short-scale equation, it can lead to undesired consequences, like the divergency of the propagation speed near the discontinuity.

The simplest physically admissible source function in the equation of u should contain a cubic nonlinearity; the dependence on both v and U can be linear. We shall concentrate upon the case when the symmetry breaking between the alternative states of the short-range

variable is weak, and causes the kinks to propagate with a speed comparable to that induced by a weak curvature with a radius far exceeding the diffusional length of the activator. This will allow us to take into account geometric factors while remaining within applicability limits of the multiscale perturbation scheme. The simplest suitable form of the model is

$$\gamma u_t = \epsilon^2 \nabla^2 u + (1 - u^2)u + \epsilon(U - v), \quad (9)$$

$$v_t = \nabla^2 v - v - \nu + \mu u. \quad (10)$$

$$U = U_0 + \frac{\beta}{\epsilon} (\langle u \rangle - 1). \quad (11)$$

With $U \leq O(1)$, eq.(9) is just the Fisher – Kolmogorov equation supplemented by an $O(\epsilon)$ symmetry-breaking term. The latter is of the right order of magnitude to balance kinetic and geometric effects in the kink propagation. Both parameters μ and β are supposed to be positive, which corresponds to the anticlinal and synclinal disposition of null isoclines, respectively, for v and U . Under these conditions, spontaneous pattern formation triggered by v is suppressed by the global variable which imitates the action of the environment in a mixed vessel. In the absence of global control ($\beta = 0$), both steady states $u_{\pm} \approx \pm 1$ are weakly excitable at $|\nu| < \mu$, while at $|\nu| > \mu$ only one state is excitable.

The dynamics of the global variable is supposed to be very fast, and to insure stable relaxation to the solution of Eq. (11). The global balance condition (11) is written in such a way that, provided $\beta = O(1)$, the value of U is large, and relaxes to an $O(1)$ level only when the upper state $u_+ \approx 1$ is prevailing, so that the fraction of the surface occupied by the lower state is at most of $O(\epsilon)$. Therefore stable patterns generated by this model at moderate values of β can only take the form of a solitary band or disk with $u < 0$ immersed in a continuum with $u > 0$. The only globally stable stationary state is, to the leading order, $u = 1$, $v = \mu - \nu$, $U = U_0$. At $\beta < \frac{1}{4}$, another pair of solutions exists, one of which is unstable and the other one is metastable.

III. EQUATION OF MOTION FOR A CURVED KINK

Problems with separated scales are generally solved using matched asymptotic expansions in the *inner* region (in the vicinity of the kink) and in the *outer* regions where one of the

alternative equilibria of the short-range variable is approached. We shall derive the equation of motion for a slowly propagating and moderately bent kink as a solvability condition that insures the existence of a stationary solution of Eq.(1) in an aligned frame comoving with the kink.

The coordinate frame aligned with a planar curve is defined in the following way. Let the curve be parametrized by a coordinate η , and its position in the plane defined as $\mathbf{x}(\eta)$. The derivatives of this function define the unit tangent vector $\mathbf{t} = \mathbf{x}'(\eta)/|\mathbf{x}'(\eta)|$ and the curvature vector $d\mathbf{t}/d\eta = \kappa\mathbf{n}$, where \mathbf{n} is the normal to the curve, and κ is the scalar curvature. By convention, the ξ axis has its origin on the curve and is directed oppositely to \mathbf{n} . The coordinate lines $\xi = \text{const}$ are obtained by shifting the curve along the normal by a constant increment; evidently, this shift causes the length to increase on convex, and to decrease on concave sections of the curve. The length element is defined as $ds^2 = d\xi^2 + (1 + \kappa\xi)^2 d\eta^2$. Accordingly, the Laplacian is expressed as

$$\nabla^2 = (1 + \kappa\xi)^{-1} \left[\partial_\xi(1 + \kappa\xi)\partial_\xi + \partial_\eta(1 + \kappa\xi)^{-1}\partial_\eta \right]. \quad (12)$$

The aligned system is well defined only sufficiently close to the curve, due to a singularity developing on the concave side at a distance of $O(\kappa^{-1})$. If the curvature radius far exceeds the the diffusional range of the short-scale variable u , the aligned system remains regular in the region where u changes between the alternative equilibria $u = u_\pm$. In the vicinity of a kink, the coordinate ξ has to be rescaled by the factor ϵ to accommodate the rapid change of u . Rescaling the tangential coordinate is not necessary as long as the curvature radius of the kink is of $O(1)$ on the extended scale, and far exceeds the kink width. Adopting this scaling, we rewrite the Laplacian Eq.(12) as

$$\nabla^2 = \epsilon^{-2}\partial_\xi^2 + \epsilon^{-1}\kappa\partial_\xi + \partial_\eta^2 - \kappa^2\xi\partial_\xi + O(\epsilon). \quad (13)$$

The time derivative is transformed in the comoving frame as $\partial_t \rightarrow \partial_t - C\epsilon^{-1}\partial_\xi$. The additional term matches the curvature term by the order of magnitude, provided the propagation velocity C is scaled as $C = \epsilon^2\gamma^{-1}c$ where $c = O(1)$. In the inner region, the long-range variable is constant across the kink in the leading order. Assuming a linear dependence on some combination w of the long-range and global variables, as e.g. in Eq. (9), we set in

Eq. (1) $f(u, v) = f_0(u) + \epsilon w f_1(u)$ where $f_0(u)$ is odd. Expanding the short-range variable as $u = u_0(\xi) + \epsilon u^{(1)}(\xi, \eta) + \dots$ yields, in the zero order

$$u_0''(\xi) + f_0(u_0) = 0. \quad (14)$$

This equation is verified by a stationary kink (antikink) solution satisfying the asymptotic condition $u_0(\xi) \rightarrow u^\pm$ at $\xi \rightarrow \pm\infty$ (for a kink) or at $\xi \rightarrow \mp\infty$ (for an antikink). In particular, for the cubic nonlinearity in Eq.(9), the kink solution is

$$u_0(\xi) = \tanh(\xi/\sqrt{2}). \quad (15)$$

The first-order equation is

$$u_{\xi\xi}^{(1)} + f_0'(u_0)u^{(1)} + \Psi(\xi, \eta) = 0, \quad (16)$$

which contains the inhomogeneity

$$\Psi(\xi, \eta) = (c + \kappa)u_0'(\xi) + f_1(u_0)w. \quad (17)$$

The propagation speed is determined by the solvability condition of Eq.(16), which implies the orthogonality of the Goldstone eigenmode $u_0'(\xi)$ of the homogeneous part, corresponding to the translational symmetry of a stationary kink or antikink, to the inhomogeneity $\Psi(\xi, \eta)$:

$$\int_{-\infty}^{\infty} u_0'(\xi)\Psi(\xi, \eta)d\xi = 0. \quad (18)$$

At $w = 0$, the well-known result $c = -\kappa$ (curvature driven motion [29]) is evident. The kink propagates along the curvature vector in such a way that a convex region occupied by one of the alternative equilibria shrinks. The lowest-order general equation of motion for a curved kink is written as

$$c(\eta) = -\kappa(\eta) \mp bw(\eta), \quad (19)$$

where

$$b = \int_{-\infty}^{\infty} u_0'(\xi)f_1(u_0(\xi)) d\xi / \int_{-\infty}^{\infty} [u_0'(\xi)]^2 d\xi. \quad (20)$$

In particular, for the model Eq.(9), $u'_0(\xi) = 2^{-1/2}\text{sech}^2(\xi/\sqrt{2})$, $f_1(u) = 1$, $w = U - v$, and $b = 3/\sqrt{2}$. The upper sign in Eq.(19) applies to a kink with the lower state prevailing at $\xi < 0$, and the lower, to an antikink with the reverse orientation.

The equation of motion Eq.(19) is closed by defining the instantaneous position of the kink in a suitable global coordinate frame and computing the local curvature. The outer equation Eq.(2) can be then solved by substituting the quasistationary values $u = u^\pm$ in the regions separated by the kink, and using Eq.(19) as a kinematic boundary condition at the kink.

IV. REGULAR STRUCTURES

A. Solitary straight kink

The simplest structure in a system with separated scales is a steadily propagating solitary straight kink. Using in Eq.(3) the quasistationary values of the short-range variable $u = u^\pm(v)$, which can be computed in the leading order in ϵ using the roots u_\pm of $f_0(u)$, and transforming to the moving frame we rewrite it as

$$\epsilon^2\gamma^{-1}c_0v_x + v_{xx} - v \pm \mu - \nu = 0, \quad (21)$$

where $\mu = \frac{1}{2}[g_0(u^+) - g_0(u^-)]$, $\nu = -\frac{1}{2}[g_0(u^+) - g_0(u^-)]$; the same form is obtained directly when the model equation (10) is used. The small parameter in the first term appears when the propagation velocity is scaled as specified in the preceding Section. Provided $\gamma \gg \epsilon^2$, the propagative term is small, and will be further omitted. Then the leading-order unperturbed solution satisfying the continuity and smoothness conditions at the kink is

$$v = \begin{cases} \mu[e^x - 1] - \nu & \text{at } x < 0, \\ \mu[1 - e^{-x}] - \nu & \text{at } x > 0. \end{cases} \quad (22)$$

When the short-scale equation (9) applies, the stationary propagation speed, defined by Eq. (19) is $c = -b[U - v(0)] = -b(U + \nu)$. The kink is at rest when the fraction of the surface occupied by the lower state, α , is $\alpha = (\epsilon/2\beta)(U_0 + \nu)$. Since this ratio is small at $\beta = O(1)$, it is likely that boundary effects have to be taken into account in this case.

B. Striped pattern

A regular striped pattern in the infinite plane with the period $2L = 2(a_+ + a_-)$ is formed by alternating straight-line kinks at $x = 2nL$ and antikinks at $x = 2(nL + a_+)$. The leading-order stationary solution for the long-range variable is

$$\begin{aligned} v &= \mu \left[2 \cosh(x - 2nL + a_-) \frac{\sinh a_+}{\sinh L} - 1 \right] - \nu \text{ at } 2(nL - a_-) < x < 2nL, \\ v &= \mu \left[1 - 2 \cosh(x - 2nL - a_+) \frac{\sinh a_-}{\sinh L} \right] - \nu \text{ at } 2nL < x < 2(nL + a_+). \end{aligned} \quad (23)$$

The equilibrium condition, that fixes the relation between the lengths a_{\pm} , is $v(0) = v(2a_+) = U$. A short computation yields

$$U + \nu = \mu \sinh(a_+ - a_-) / \sinh(a_+ + a_-). \quad (24)$$

Using also Eq. (11) we obtain

$$U_0 + \nu = \mu \frac{\sinh(a_+ - a_-)}{\sinh(a_+ + a_-)} + \frac{2\beta a_-}{\epsilon(a_+ + a_-)}. \quad (25)$$

Evidently, $a_+ \gg a_-$, unless $\beta \leq O(\epsilon)$.

C. Solitary band

A solution in the form of a solitary band with $u < 0$ immersed in a continuum with $u > 0$ can be obtained from Eq. (23) in the limit $a_+ \rightarrow \infty$. The solution, that satisfies the continuity and smoothness conditions at the kink and the antikink located at $x = \pm a$, is

$$v = \begin{cases} \mu(2e^{-a} \cosh x - 1) - \nu & \text{at } |x| < a, \\ \mu(1 - 2e^{-|x|} \sinh a) - \nu & \text{at } |x| > a. \end{cases} \quad (26)$$

Some typical profiles of v are shown in Fig. 2a. The stationarity condition is

$$\nu + U = \mu e^{-2a}. \quad (27)$$

Solitary structures naturally appear at $\beta = O(1)$. Since the interaction between distant kinks is exponentially small, one can also envisage a pattern consisting of N well separated parallel bands. When such a structure is placed on a plate with the width L/ϵ , the fraction

of the surface occupied by the lower state is $\alpha = 2\epsilon Na/L$. Then $U = U_0 - 2\beta_1 a$, where $\beta_1 = 2N\beta a/L$. It is easy to see that U_0 can be compensated by a shift of ν ; further on, we shall set it therefore to zero. Then the stationarity condition Eq. (27) can be written in the form

$$\nu - 2\beta_1 a = \mu e^{-2a}, \quad (28)$$

If this equation is solved graphically, stable solutions can be obtained only when the *absolute value* of slope of the straight line representing the left-hand side is *less* than that of the right-hand side at the intersection point. The necessary condition for the existence of such solutions is $\beta_1 \leq \mu$. Within the parametric range $\mu > \beta_1 > 0$, $\mu > \nu > \nu_c \equiv \beta_1[1 - \ln(\beta_1/\mu)]$, there are two solutions, of which one corresponding to a smaller width is stable according to the above criterion. The largest possible width, achieved at $\nu = \nu_c$, is $a = \frac{1}{2} \ln(\mu/\beta_1)$.

D. Solitary disk

In 2d, the kink should acquire a circular shape due to the “line tension”, and the stationary solution depends only on the long-range radial coordinate r . The stationary outer equation is

$$v_{rr} + r^{-1}v_r - v - \nu \pm \mu = 0, \quad (29)$$

The stationary solution for a disk with $u < 0$ immersed in a continuum with $u > 0$, satisfying the continuity and smoothness conditions at the kink located at $r = a$, is

$$v = \begin{cases} \mu[2aK_1(a)I_0(r) - 1] - \nu & \text{at } r < a, \\ \mu[1 - 2aI_1(a)K_0(r)] - \nu & \text{at } r > a, \end{cases} \quad (30)$$

where I_n , K_n are modified Bessel functions. The identity $K_1(a)I_0(a) + K_0(a)I_1(a) = a^{-1}$ should be used when the boundary conditions are checked. Some profiles of v are shown in Fig. 2b. One can notice that the value of the long-range variable at the kink location is shifted upwards to compensate the curvature-driven shrinking action; this shift grows with the decreasing disk radius.

Using $v(a)$ and $\kappa = a^{-1}$ in Eq.(19) yields the stationarity condition

$$U + \nu = -(ba)^{-1} + \mu a [K_1(a) I_0(a) - K_0(a) I_1(a)]. \quad (31)$$

If a pattern consisting of N well separated disks is formed on a plate with the surface area $(L/\epsilon)^2$, the fraction of the surface occupied by the lower state is $\alpha = \epsilon\pi N(a/L)^2$. Then $U = U_0 - 2\pi\beta N(a/L)^2$, (where U_0 can be again set to zero), and the stationarity condition Eq. (31) can be written, using the parameter $\beta_2 = \pi\epsilon N\beta/L^2$, in the form

$$\nu a + b^{-1} = 2\beta_2 a^3 + \mu a^2 [K_1(a) I_0(a) - K_0(a) I_1(a)]. \quad (32)$$

If this equation is solved graphically (Fig. 3), the slope of the left-hand side of this equation at the intersection point corresponding to a stable solution should be *algebraically larger* than the slope of the right-hand side. When it is so, the effective repulsive action due to the long-range field decreases with growing radius faster than the shrinking action due to the line tension. Whenever Eq.(31) has a single solution, this solution should be unstable. When an additional pair of solutions bifurcates at a tangent point, one of these solutions is stable according to the above criterion. Further stability analysis is found in the next Section.

V. STABILITY OF REGULAR STRUCTURES

The “naive” stability criteria in the preceding Section refer only to the stability to perturbations that do not reduce the symmetry of the problem. In this Section, we shall investigate stability to asymmetric perturbations. Perturbations of this kind do not change the fraction of the surface occupied by either state, and therefore do not involve the global control variable. Throughout this Section, we shall assume that γ is not exceedingly small, i.e. $\gamma \geq O(\epsilon)$. Under this condition, the distribution of the long-range variable follows slow shifts of the kink position quasistationarily, unless at distances that are large even on the extended scale.

A. Stability of a solitary straight kink

We shall now apply the equation of motion Eq.(19) to the problem of stability of a solitary straight kink to infinitesimal perturbations. The suitable global coordinate frame for this problem is a Cartesian frame (x, y) comoving with the unperturbed kink. Denoting the instantaneous position of the kink relative to its unperturbed position as $x = \zeta(y, t)$, we take note that, as long as the amplitude of the perturbation is much smaller than its wavelength, the normal vector, defining the direction of the kink propagation, is almost parallel to the x axis, and the propagation speed is expressed as $\zeta_t = \epsilon^2 \gamma^{-1} c$. In the same approximation, the curvature is given by $\kappa = -\zeta_{yy}$. Expanding also the long-range variable in the vicinity of the unperturbed position, we reduce Eq.(19) to the form

$$\zeta_\tau = \zeta_{yy} + b[V(0, y, \tau) + v'_s(0)\zeta]. \quad (33)$$

Here $v'_s(0) = \mu$ is the stationary flux at the kink following from Eq.(22), V is the perturbation of the long-range variable, and $\tau = \epsilon^2 \gamma^{-1} t$ is the rescaled time variable.

The correction to v due to a weak perturbation of the kink can be computed in a simple way by observing that any shift of the kink position by an infinitesimal increment ζ is equivalent to switching the sign of the source term in Eq.(10) in a narrow region near $x = 0$. This approach is akin to the ‘‘singular limit eigenvalue’’ method applied earlier to the stability analysis of kinks in one dimension [30]. Although the perturbation ξ is habitually presumed to be arbitrarily small for the purpose of linear stability analysis, the method is actually applicable also to finite perturbations of the kink position, provided they are small on the extended scale, i.e. $\zeta \leq O(\epsilon)$.

At $\gamma \geq O(\epsilon)$, the quasistationary form of the perturbation equation is applicable:

$$\nabla^2 V - V = 2\mu\zeta(y, t)\delta(x). \quad (34)$$

In a standard way, we are looking for a solution in a spectral form

$$\zeta(y, \tau) = \chi(k, \lambda)e^{\lambda\tau + ik y}, \quad V(x, y, \tau) = \psi(x; k, \lambda)e^{\lambda\tau + ik y}. \quad (35)$$

The dispersion relation $\lambda(k^2)$ determines the stability to infinitesimal perturbations. Using Eq. (35) in Eq.(34) yields

$$\psi_{xx} - q^2\psi = 2\mu\zeta(y, t)\delta(x), \quad (36)$$

where $q^2 = 1 + k^2$. The solution of this equation is

$$\psi(x) = -\mu\chi(k, \lambda)q^{-1}e^{-q|x|}. \quad (37)$$

Using Eqs.(22), (35), (37) in Eq.(33) yields the dispersion relation

$$\lambda = -k^2 + b\mu(1 - q^{-1}). \quad (38)$$

The eigenvalues $\lambda(k^2)$ are always real, and, as expected, λ vanishes at $k = 0$, which reflects the translational symmetry of the kink. The loss of stability to long-scale perturbations occurs when the derivative $d\lambda/d(k^2)$ at $k = 0$ becomes positive. This happens at $b\mu > 2$. Since the function $\lambda(k^2)$ is convex, the loss of stability always occurs with growing μ in the long-scale mode.

B. Stability of a solitary band

The equations of motion for infinitesimal displacements $\zeta^{(1)}$, $\zeta^{(2)}$ of the kink at $x = a$ and the antikink at $x = -a$ that confine a solitary band (Section IV C) are written analogous to Eq.(33). We take note that opposite signs appear in the equations of motion Eq. (19) for the kink and the antikink. Using the expression for the stationary fluxes following from Eq.(26), we obtain

$$\zeta_\tau^{(j)} = \zeta_{yy}^{(j)} + b \left[\pm V(\pm a, y, \tau) + \mu(1 - e^{-2a})\zeta^{(j)} \right]. \quad (39)$$

It is advantageous to consider the symmetric and antisymmetric combinations of the displacements, $\zeta^\pm = \frac{1}{2}(\zeta^{(1)} \pm \zeta^{(2)})$, that may lead, respectively, to *zigzag* or *varicose* instabilities. It is clear from Eq.(39) that ζ^\pm are coupled, respectively, to the antisymmetric and symmetric parts V^\mp of the perturbation field V :

$$\zeta_\tau^\pm = \zeta_{yy}^\pm + b \left[V^\mp(a, y, \tau) + \mu(1 - e^{-2a})\zeta^\pm \right]. \quad (40)$$

The quasistationary equations for both perturbation fields, V^\mp , are identical:

$$\nabla^2 V^\mp - V^\mp = 2\mu\zeta^\pm(y, \tau)\delta(x - a). \quad (41)$$

Setting as before $V^\pm = \psi^\pm e^{\lambda\tau + ik y}$, $\zeta^\pm = \chi^\pm e^{\lambda\tau + ik y}$ yields

$$\psi^+(x) = \begin{cases} -2\mu\chi^+ q^{-1} e^{-qa} \cosh qx & \text{at } |x| < a, \\ -2\mu\chi^+ q^{-1} e^{-q|x|} \cosh qa & \text{at } |x| > a, \end{cases} \quad (42)$$

$$\psi^-(x) = \begin{cases} -2\mu\chi^- q^{-1} e^{-qa} \sinh qx & \text{at } |x| < a, \\ -2 \operatorname{sign}(x) \mu\chi^- q^{-1} e^{-q|x|} \sinh qa & \text{at } |x| > a. \end{cases} \quad (43)$$

The zigzag and varicose branches of the dispersion relation are given by

$$\begin{aligned} \lambda^+ &= -k^2 + b\mu \left[1 - e^{-2a} - q^{-1} (1 - e^{-2qa}) \right], \\ \lambda^- &= -k^2 + b\mu \left[1 - e^{-2a} - q^{-1} (1 + e^{-2qa}) \right]. \end{aligned} \quad (44)$$

Vanishing λ^- at $k = 0$ reflects the translational symmetry of the band. Due to convexity of the function $\lambda^-(k^2)$, the loss of stability first occurs at $k = 0$. The solution is unstable when the derivative $d\lambda^-/dk$ at $k = 0$ is positive. The critical point of the long-scale zigzag instability is

$$\mu = \frac{2/b}{(1 + 2a)e^{-2qa} - 1}. \quad (45)$$

The varicose branch, $\lambda^+(k^2)$ lies persistently lower than the zigzag one. Thus, the stability limit is always given by Eq.(45). The most dangerous perturbation corresponds to the long-wave limit $k \rightarrow 0$, i.e. $q \rightarrow 1$. The limit of the zigzag instability is shifted to higher values of μ with a decreasing band thickness.

C. Stability of a solitary disk

In order to check stability of the stationary solution that has the form of a solitary disk with the radius a , as in Section IV D, we use the cylindrical coordinates (r, ϕ) , and set $r = a[1 + \zeta(\phi, t)]$, where $\zeta(\phi, t) \ll 1$. The curvature of the kink is expressed as $\kappa = a^{-1}(1 - \zeta - \zeta_{\phi\phi})$. Expanding, as before, the long-range variable in the vicinity of the unperturbed position brings Eq.(19) to the form

$$\zeta_\tau = a^{-2} (\zeta_{\phi\phi} + \zeta) + b \left[a^{-1} V(0, \phi, \tau) + v'_s(0)\zeta \right], \quad (46)$$

where $v'_s(0) = 2\mu a I_1(a) K_1(a)$ is the stationary flux at the kink following from Eq.(30). The quasistationary equation for the perturbation field V is

$$\nabla^2 V - V = 2\mu a \zeta(\phi, t) \delta(r - a). \quad (47)$$

We are looking for a solution in the form

$$\zeta(\phi, \tau) = \chi_n e^{\lambda_n \tau + i n \phi}, \quad V(r, \phi, \tau) = \psi(r; n) e^{\lambda_n \tau + i n \phi}, \quad (48)$$

where n is an integer. The equation of ψ is

$$\psi_{rr} + \frac{1}{r} \psi_r - \left(1 + \frac{n^2}{r^2}\right) \psi = 2\mu a \chi_n \delta(r - a). \quad (49)$$

The solution of this equation is

$$\psi(r) = \begin{cases} -2\mu a^2 K_n(a) I_n(r) & \text{at } r < a, \\ -2\mu a^2 I_n(a) K_n(r) & \text{at } r > a. \end{cases} \quad (50)$$

Using Eqs.(30), (48), (50) in Eq.(33) yields the dispersion relation

$$\lambda_n = -(n^2 - 1)/a^2 + b\mu a [I_1(a) K_1(a) - I_n(a) K_n(a)]. \quad (51)$$

As expected, λ_n vanishes at $n = 1$, which corresponds to a shift of the disk without deformation. One can check numerically that, of all angular modes, the quadrupole mode $n = 2$, deforming the disk into an ellipse, is the most dangerous one. At large a , this can be seen by using the asymptotics of Bessel functions to compute the asymptotic value of μ at the instability threshold

$$\mu_c(n) = \frac{(n^2 - 1)/b}{\frac{1}{4} \left[\Gamma\left(\frac{3}{2} + n\right) / \Gamma\left(-\frac{1}{2} + n\right) \right]^2 - \frac{9}{64}}, \quad (52)$$

where $\Gamma(x)$ is the gamma-function. The asymptotic limiting value increases with n at $n > 2$.

D. Stability of a striped pattern

A quasistationary perturbation V of the long-range field in alternating regions of a striped pattern with the period $2L$ (Section IV B) due to displacements of respective kinks at $x = 2nL$ by $\zeta^{(1,n)}$ and antikinks at $x = 2(nL + a_+)$ by $\zeta^{(2,n)}$ obeys the equation

$$\nabla^2 V - V = 2\mu \sum_n (-1)^n \left[\zeta^{(1,n)} \delta(x - 2nL) - \zeta^{(2,n)} \delta(x - 2nL - 2a_+) \right]. \quad (53)$$

The equation of motion of the kinks is obtained, analogous to Eq.(33), by using in Eq.(19) $v = v'_s(2nL)\zeta^{(n)} + V(2nL, y, \tau)$, where $v'_s(2nL) \equiv J = 2\mu \sinh a_+ \sinh a_- / \sinh L$ is the stationary flux following from Eq.(23); at the antikink locations, $x = 2(nL + a_+)$, $v'_s(2nL) = -J$, and the respective values enter the equation of motion with the reverse sign:

$$\begin{aligned} \zeta_\tau^{(1,n)} &= \zeta_{yy}^{(1,n)} + b \left[J\zeta^{(1,n)} + V(2nL, y, \tau) \right], \\ \zeta_\tau^{(2,n)} &= \zeta_{yy}^{(2,n)} + b \left[J\zeta^{(2,n)} - V(2nL + 2a_+, y, \tau) \right]. \end{aligned} \quad (54)$$

Presenting the perturbation V in each successive stripe with a prevailing positive or negative state of the short-scale variable as $V^{(j,n)} = \psi^{(j,n)} e^{\lambda\tau + iky}$, and kink displacements as $\zeta^{(j,n)} = \chi^{(j,n)} e^{\lambda\tau + iky}$, $j = 1, 2$, we write the equation of the spectral components

$$\psi_{xx}^{(j,n)} - q^2 \psi^{(j,n)} = 0. \quad (55)$$

The matching conditions, taking into account localized perturbations due to displacements of respective kinks and antikinks, are

$$\begin{aligned} \psi^{(1,n)} &= \psi^{(2,n)}, \quad \psi_x^{(1,n)} - \psi_x^{(2,n)} = 2\mu\chi^{(1,n)} \quad \text{at } x = 2nL, \\ \psi^{(1,n)} &= \psi^{(2,n+1)}, \quad \psi_x^{(1,n)} - \psi_x^{(2,n+1)} = 2\mu\chi^{(2,n)} \quad \text{at } x = 2(nL + a_+). \end{aligned} \quad (56)$$

The solution of Eq.(55) is expressed as

$$\psi^{(j,n)} = A^{(j,n)} e^{qx} + B^{(j,n)} e^{-qx}, \quad (57)$$

We shall define the coefficients in the above expression, as well as the displacements at particular locations, through respective generating functions:

$$\begin{aligned} \alpha_j(z) &= \sum_{n=-\infty}^{\infty} A^{(j,n)} e^{(iz+2qL)n}, \quad \beta_j(z) = \sum_{n=-\infty}^{\infty} B^{(j,n)} e^{(iz-2qL)n}, \\ \gamma_j(z) &= \sum_{n=-\infty}^{\infty} \chi^{(j,n)} e^{izn}, \quad j = 1, 2. \end{aligned} \quad (58)$$

Multiplying the matching conditions Eq.(56) by e^{izn} and summing over n yields a set of equations for $\alpha_j(z)$, $\beta_j(z)$:

$$\begin{aligned}
\alpha_1(z) - \alpha_2(z) + \beta_1(z) - \beta_2(z) &= 0, \\
\alpha_1(z) - \alpha_2(z) - \beta_1(z) + \beta_2(z) &= 2\mu q^{-1}\gamma_1(z), \\
e^{2qa_+}\alpha_1(z) - e^{-(iz+2qa_-)}\alpha_2(z) + e^{-2qa_+}\beta_1(z) - e^{-(iz-2qa_-)}\beta_2(z) &= 0, \\
e^{2qa_+}\alpha_1(z) - e^{-(iz+2qa_-)}\alpha_2(z) - e^{-2qa_+}\beta_1(z) + e^{-(iz-2qa_-)}\beta_2(z) &= 2\mu q^{-1}\gamma_2(z). \tag{59}
\end{aligned}$$

Two more equations are obtained in the same way from Eq.(54):

$$\begin{aligned}
(\lambda + k^2 - bJ)\gamma_1(z) &= \alpha_1(z) + \beta_1(z), \\
(\lambda + k^2 - bJ)\gamma_2(z) &= -e^{2qa_+}\alpha_1(z) - e^{-2qa_+}\beta_1(z). \tag{60}
\end{aligned}$$

The general dispersion relation, obtained as the condition that Eqs. (59), (60) have a non-trivial solution, is quite cumbersome. As in Section VB, it is convenient to work with zigzag and varicose modes, that correspond, respectively, to like and opposite signs of displacements of adjacent kinks and antikinks. These modes, obtained by introducing the symmetric and antisymmetric combinations $\gamma^\pm = \frac{1}{2}(\gamma_1 \pm \gamma_2)$, decouple, however, only at $z = 0$. The symmetric (zigzag) and antisymmetric (varicose) branches of the dispersion relation at $z = 0$ are computed as

$$\begin{aligned}
\lambda^+ &= -k^2 + 2b\mu \left(\frac{\sinh a_+ \sinh a_-}{\sinh L} - \frac{\sinh qa_+ \sinh qa_-}{q \sinh qL} \right), \\
\lambda^- &= -k^2 + 2b\mu \left(\frac{\sinh a_+ \sinh a_-}{\sinh L} - \frac{\cosh qa_+ \cosh qa_-}{q \sinh qL} \right). \tag{61}
\end{aligned}$$

The varicose branch $\lambda^-(k^2)$ lies persistently lower than $\lambda^+(k^2)$, and therefore can be disregarded. Vanishing λ^+ at $k = 0$ reflects the translational symmetry of the entire pattern. The loss of stability in the long-scale zigzag mode occurs when the derivative $\partial\lambda^+/\partial(k^2)$ at $k = 0$ vanishes.

A simpler form of the dispersion relation is obtained at $\nu = 0$ when the striped pattern is symmetric, with $a^+ = a^- = L$. The zigzag branch of the dispersion relation is

$$\lambda = -k^2 + b\mu \left[\tanh L - \frac{q^{-1} \tanh qL}{1 - \sin^2 \frac{z}{2} (1 - \tanh^2 qL)} \right]. \tag{62}$$

One can clearly see here that λ decreases monotonically with growing z , so that when μ increases the loss of stability always occurs in a concerted long-scale zigzag mode $z = 0$.

Again, the bracketed expression in Eq.(62) is a convex function of k^2 , and therefore the loss of stability should first occur at $k = 0$. The instability limit shifts to larger μ as the wavelength decreases, as shown in Fig. 4. In the other limit, $a^+ \gg a^-$, Eq. (61) reduces to the dispersion relation for a solitary band, Eq. (44).

VI. DISCUSSION

Although both the zigzag instability of the solitary band solution and the quadrupole instability of the solitary disk are not coupled to the global control parameter β , the stability boundary in the parametric plane (μ, ν) depends on the global parameter as well because of the parametric dependence of the stationary solution. The existence and stability regions of the solitary band solution are shown in Fig. 5. In the absence of global control, the solution exists in the entire triangle $\mu > \nu > 0$, but suffers zigzag instability to the right of the dashed line departing from the μ axis. Both the existence and stability limits shift upwards as the parameter β_1 increases.

The existence and stability regions of the solitary disk solution are shown in Fig. 6. At $\beta_2 = 0$, the tip of the existence region penetrates into the half-plane $\nu < 0$; at $\mu > b^{-1}$, the lower boundary of the existence region coincides with the axis $\nu = 0$. Two other cusped curves, drawn for $\beta_2 = 10^{-2}$ (Fig. 6a) and $\beta_2 = 10^{-3}$ (Fig. 6b), bear witness that the existence conditions are very sensitive to small changes of the global parameter β_2 . This sensitivity is, indeed, essential, since the definition of the parameter β_2 includes the small parameter ϵ , and therefore β_2 (or, at least, the ratio β_2/β_1) should be small. The limits of the quadrupole instability are shown in the same picture by dashed lines (at $\beta_2 = 10^{-3}$, the instability limit is outside the depicted region).

The regions where either or both band and disk solutions can appear are shown together in Fig. 7. The coexistence region is most extensive when there is no global control (Fig. 7a,b). One can recall that coexistent striped and dotted patterns (which can be viewed as arrays of band or disk structures) were also found experimentally [11]. A narrower coexistence region is seen in Fig. 7c, where the region of *stable* solitary disk solutions at $\beta_2 = 10^{-3}$, bounded by the solid cusped line, is shown together with dashed lines representing the lower bounds

of the existence of *stable* solitary band solutions at several values of β_1 . The coexistence region shrinks with increasing global control very fast, as the limit of the zigzag instability of solitary band solutions shifts to the left and upwards, and at the same time the tip of the cusped region of stable disk solutions retreats to higher values of both μ and ν .

This picture is in qualitative agreement with the results of the computer experiment by Middy and Luss [15], although in the latter work there was no separation between characteristic scales of both local variables. In runs without global control, Middy and Luss observed, depending on initial conditions, either bands or disks. Although typically a large number of either objects were present, they could be seen, essentially, as solitary structures, since the diffusivity of both local variables was small, and therefore separated kinks could interact only very weakly. With the increasing global control parameter, the number of either bands or disks decreased, and some bands disintegrated into a number of disks, apparently, due to zigzag instability.

One should recall that the global control parameter β_1 or β_2 , as defined above, is proportional to the number of “solitary” objects N . Therefore decreasing N brings the system back into the parametric region where the remaining solitary structures can be sustained. If the values of μ and ν correspond to the parametric region where both bands and disks are stable without global control, bands typically disappear first as the global control becomes stronger. Subsequently, the sustainable number of disks decreases, and, eventually, inhomogeneous solutions disappear altogether, in agreement with the observations by Middy and Luss.

ACKNOWLEDGMENTS

This work has been supported by the Fund for Promotion of Research at the Technion. I thank Dan Luss for stimulating discussions, and for acquainting me with Ref. [15] prior to publication.

REFERENCES

- [1] Y. Kuramoto, *Chemical Waves, Oscillations and Turbulence* (Springer, New York, 1984).
- [2] R.J. Field and M. Burger *Oscillations and Travelling Waves in Chemical Systems*, (J.Wiley, New York, 1985).
- [3] J.D. Murray, *Mathematical Biology* (Springer, Berlin, 1989)
- [4] S. Chandrasekhar, *Hydrodynamic and Hydromagnetic stability* (Oxford U.P. 1961).
- [5] M.C. Cross and P.C. Hohenberg, Rev. Mod. Phys. **65** 851 (1993).
- [6] S.G. Müller, T. Plesser, and B. Hess, Naturwissenschaften **71** 637 (1984)
- [7] W.Y. Tam, J.A. Vastano, H.L.Swinney, and W. Horsthemke, Phys. Rev. Lett. **61** 2163 (1988).
- [8] J. Elezgaray and A. Arneodo, J. Chem. Phys. **95** 323 (1991)
- [9] V. Castets, E. Dulos, J. Boissonade, and P. De Kepper, Phys. Rev. Lett. **64** 2953 (1990).
- [10] Q. Ouyang, and H.L.Swinney, Chaos **1** 411 (1991).
- [11] Q. Ouyang, Z. Nosticzius, and H.L.Swinney, J. Phys. Chem. **96** 6773 (1992).
- [12] K.J. Lee, W.D. McCormick, Q. Ouyang, and H.L.Swinney, Science **261** 192 (1993).
- [13] S. Jakubith, H.H. Rotermund, W. Engel, A. Vonoertzen, and G. Ertl, Phys. Rev. Lett. **65** 3013 (1990).
- [14] J.E. Pearson, Science **261** 189 (1993).
- [15] U. Middy and D. Luss, J. Chem. Phys., to appear (1994).
- [16] L. Segel and J.L. Jackson, J. Theor. Biol.**37** 545 (1972).
- [17] P.C. Fife, *Mathematical Aspects of Reacting and Diffusing Systems*, (Springer, Berlin, 1979).

- [18] L.M. Pismen, J. Chem. Phys. **71** 462 (1979).
- [19] G.A. Gordonier, F. Schuth, and L.D. Schmidt, J. Chem. Phys. **91** 5374 (1989).
- [20] G. Philippou, F. Schulz, and D. Luss, J. Chem. Phys. **95** 3224 (1991).
- [21] L.M. Pismen, Chem. Eng. Sci. **34** 563 (1979).
- [22] O.Lev, M.Sheintuch, L.M.Pismen, and Ch.Yarnitzky, Nature, **336** 458 (1988).
- [23] O. Lev, M. Sheintuch, Ch. Yarnitzky, and L.M. Pismen, Chem. Eng. Sci., **45** 839 (1990).
- [24] H. Willebrand, T.Hüntler, F.J. Niedernostheide, R. Dohmen, and H.-G. Purwins, Phys. Rev. **A45** 8766 (1992).
- [25] U. Middy, M.D. Graham, D. Luss, and M. Sheintuch, J. Chem. Phys. **98** 2823 (1993).
- [26] H. Levine and X. Zou, Phys. Rev. Lett. **69** 204 (1992).
- [27] T. Ohta, M. Mimura, and R. Kobayashi, Physica **D34** 115 (1989).
- [28] J.W. Cahn, Acta Metall. **9** 795 (1961)
- [29] J. Rubinstein, P. Sternberg and J.B. Keller, SIAM J. Appl. Math. **49**, 116 (1989).
- [30] Y. Nishiura and M. Mimura, SIAM J. Appl. Math. **49**, 481 (1989).

FIGURES

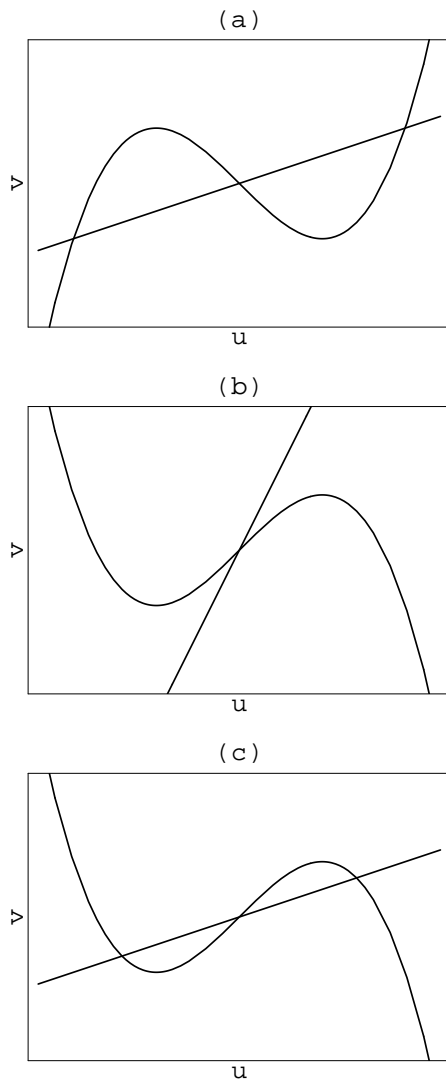


FIG. 1. Synclinal (a) and anticlinal (b,c) disposition of null isoclines.

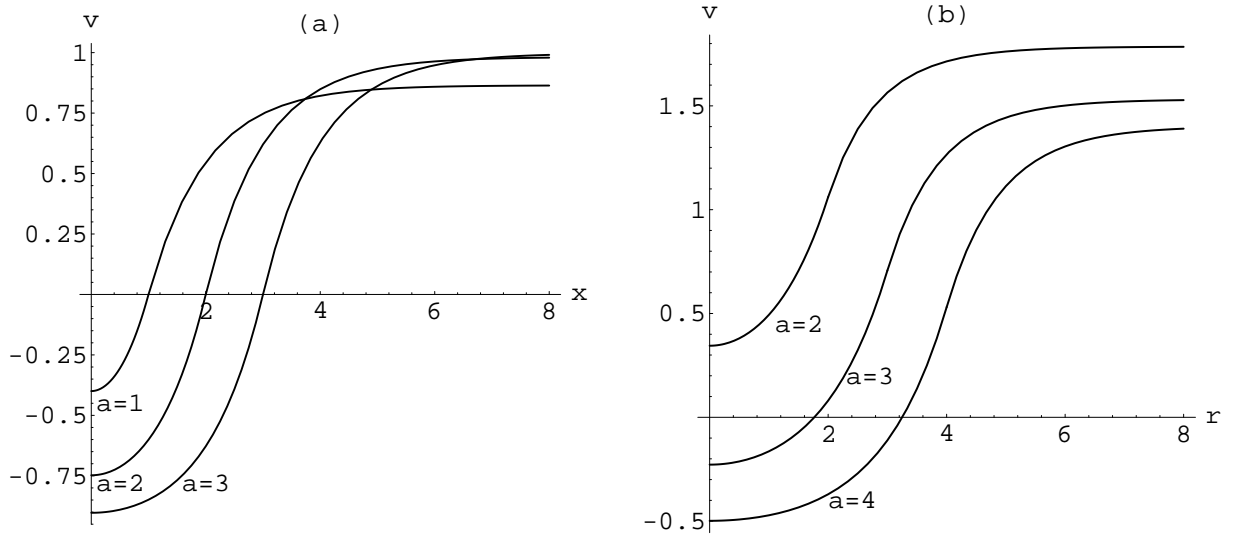


FIG. 2. The profile of the long-range variable v for a solitary band (a) and disk (b) solutions. The value of v is normalized by μ , and the value of the parameter ν is chosen in such a way that the bounding kink is stationary in the absence of global control. The curves are marked by the values of the band half-width or the disk radius a .

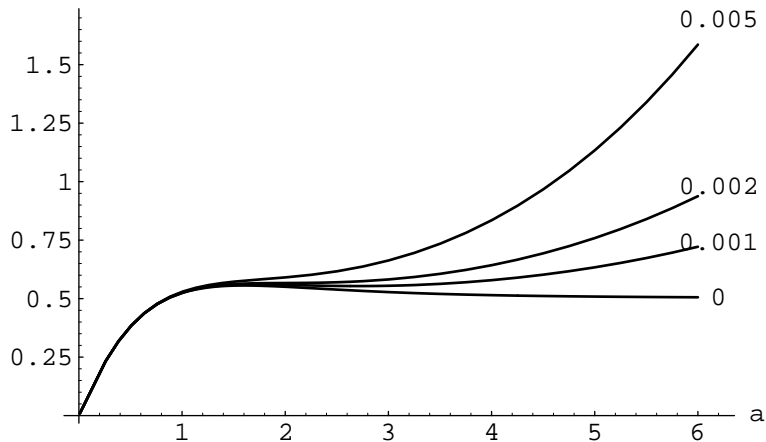


FIG. 3. Construction of stationary solitary disk solutions. Each curve presents the plot of the r.h.s. of Eq. (32), and is marked by the appropriate value of the global control parameter β_2 . Solutions are obtained as intersection points with straight lines presenting the l.h.s. of Eq. (32).

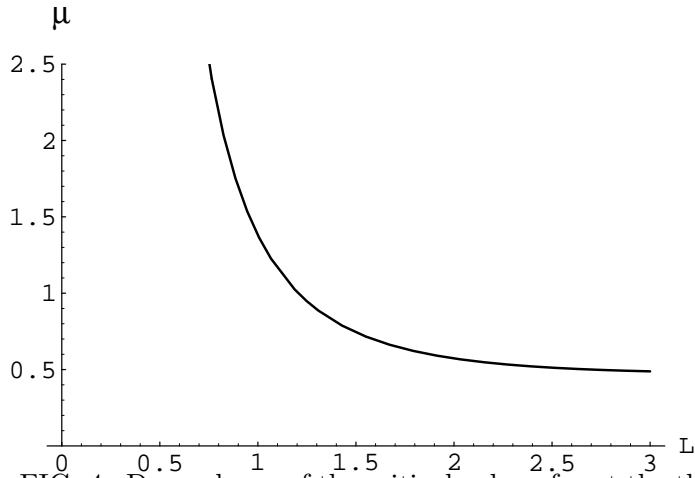


FIG. 4. Dependence of the critical value of μ at the threshold of the long-scale concerted zigzag instability of a symmetric striped pattern on the half-period L .

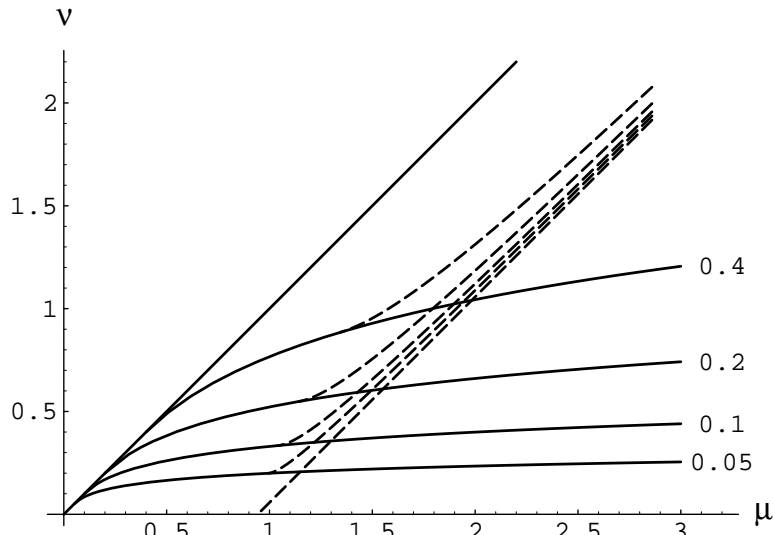


FIG. 5. Existence and stability regions of the solitary band solution in the parametric plane (μ, ν) . The solution exists in the region bounded by the diagonal $\nu = \mu$ and the solid line marked by an appropriate value of the global control parameter β_1 . Dashed lines denote the limits of the zigzag instability at the same values of the parameter β_1 .

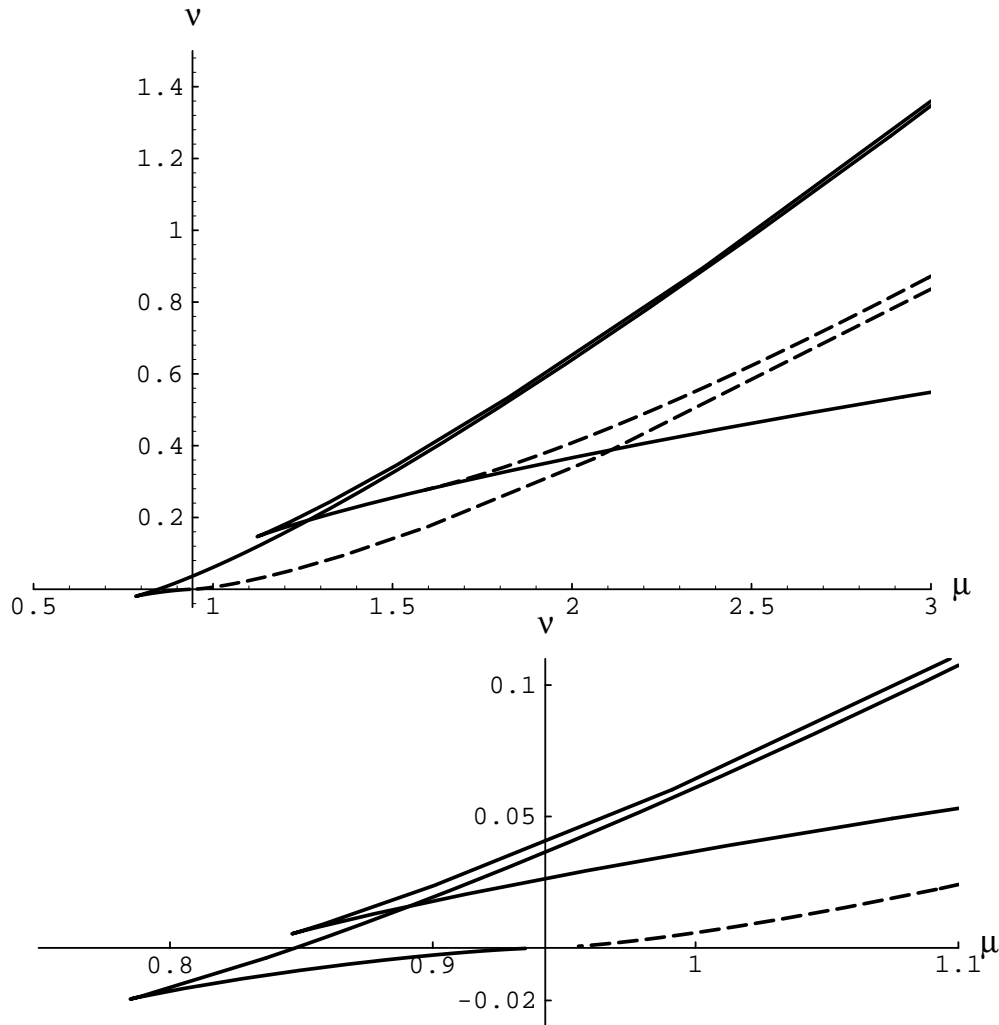


FIG. 6. Existence and stability regions of the solitary disk solution in the parametric plane (μ, ν) for the values of the global control parameter $\beta_2 = 0$, $\beta_2 = 10^{-2}$ (a) and $\beta_2 = 0$, $\beta_2 = 10^{-3}$ (b). Dashed lines denote the instability limits in the quadrupole mode. At $\beta_2 = 10^{-3}$, the instability limit is outside the depicted region.

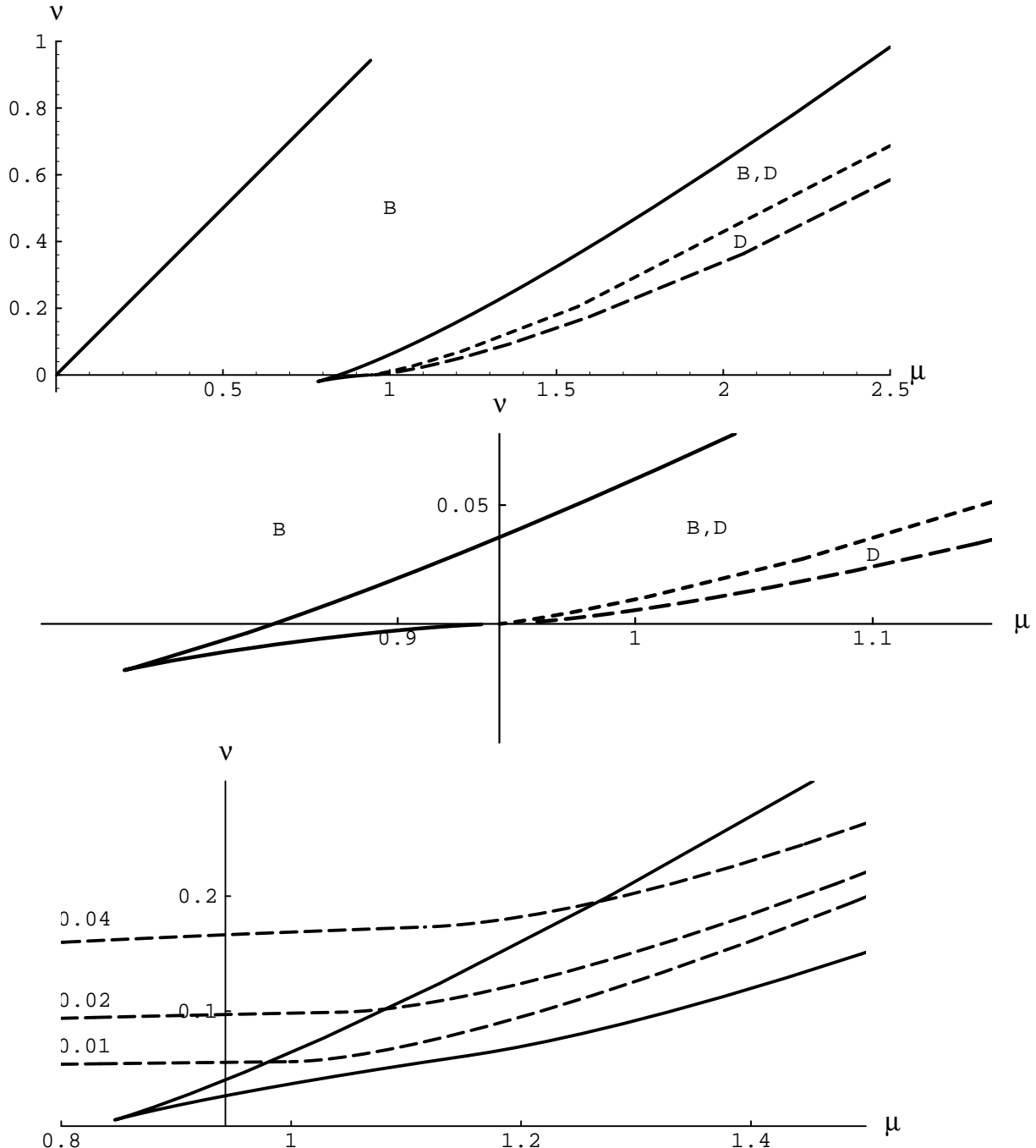


FIG. 7. Comparison of the existence and stability regions of the solitary band (B) and disk (D) solutions in the parametric plane (μ, ν) for the values of the global control parameter $\beta_1 = \beta_2 = 0$ (a,b), and $\beta_2 = 10^{-3}$ (c). In (a,b), solid lines denote the bounds of existence, and dashed lines, the stability limits of both the band and the disk solutions. The region adjacent to the cusp is shown on a larger scale in (b). The solid cusped curve in (c) shows the existence bounds of stable solitary disk solutions at $\beta_2 = 10^{-3}$. The dashed lines in (c) denote the existence bounds of stable solitary band solutions, and are marked by the appropriate values of β_1 .